Can we really solve an arch stability problem?

Jacek Chróścielewski [a], Victor A. Eremeyev [a,b,*]

[a] *Faculty of Civil and Environmental Engineering, Gdańsk University of Technology, ul. Gabriela Narutowicza 11/12 80-233 Gdańsk, Poland*
[b] *Department of Civil and Environmental Engineering and Architecture (DICAAR), University of Cagliari, Via Marengo, 2, 09123 Cagliari, Italy*

A R T I C L E   I N F O

A B S T R A C T

We bring attention to the problem of solving nonlinear boundary-value problems for elastic structures such as arches and shells. Here we discuss a classical problem of a shear-deformable arch postbuckling. Considering a postbuckling behaviour of a circular arch we discuss the possibility to find numerically a solution for highly nonlinear regimes. The main attention is paid to the problem of determination of all solutions. The main conclusion that there is no guarantee to find all solutions, in general.

1. Introduction

After famous Euler's elastica problem stability and postbuckling analysis became a very developed branch of structural mechanics. In this field hundreds of books and thousand of papers were published, see e.g. Amabili (2008), Antman (2005), Bažant and Cedolin (1990), Luongo, Ferretti, and Di Nino (2023), Perelmuter and Slivker (2013), Thompson and Hunt (1973), Timoshenko and Gere (1963) and Wang, Wang, and Reddy (2005) and the references therein. Nevertheless, the buckling and especially postbuckling analysis is still topical, see e.g. recent works by Barretta, Čanadija, Luciano, and de Sciarra (2022), Chen, Wang, and Yan (2023), Civalek, Uzun, and Yaylı (2023), Darban, Luciano, Caporale, and Fabbrocino (2020), Dehrouyeh-Semnani (2021), Epstein and Javadi (2023), Gholipour and Ghayesh (2020), Kapitaniak, Vaziri, and Wiercigroch (2020), Ong, Ghayesh, and Losic (2023), Penna (2023), Rezaiee-Pajand and Rajabzadeh-Safaei (2022), Taloni, Vilone, and Ruta (2023), Vaccaro (2022), Wang et al. (2023) and Yang, Wang, Kang, Yu, and Li (2023) for beams and Dastjerdi, Alibakhshi, Akgöz, and Civalek (2023), Khaniki and Ghayesh (2023), Malikan, Krasheninnikov, and Eremeyev (2020), Roudbari, Jorshari, Lü, Ansari, Kouzani et al. (2022), Wang, Liu, Fu, Zhang, Wang et al. (2021) and Yee and Ghayesh (2023) for shells. This relates to both appearance of new materials such as beam-lattice metamaterials or origami/kirigami structures (Choudhury, 2022; dell'Isola & Steigmann, 2020; Lakes, 2020; Peraza Hernandez, Hartl, & Lagoudas, 2019) as well as extensions of classic models of continua and structures considering various phenomena as long-range interactions and size-effects observed at small scales. Stability-related problems mostly corresponded to such flexible structures as beams, arches, trusses, plates, and shells. In particular, curved thin-walled structures, i.e. arches and shells, may demonstrate a rather complex behaviour in highly nonlinear regimes including existence of multiple solutions. This results in the necessity of developing efficient numerical tools as well as further mathematical analysis. Unfortunately, determination of all solutions or at least a number of possible solutions within discrete or continuum models constitute a rather complex problem. In the literature one can find a few results related to a priori determination of a number of possible solutions, see e.g. Vorovich (1998) for shallow shells where nonlinear functional analysis was applied.

This paper deals with the general problem of determining the equilibrium configurations of structures in the pre- and postbuckling range of deformation including snap-through, snap-back, and other bifurcation phenomena. The aim of this paper is to highlight

---

* Corresponding author at: Department of Civil and Environmental Engineering and Architecture (DICAAR), University of Cagliari, Via Marengo, 2, 09123 Cagliari, Italy.
E-mail addresses: jchrost@pg.edu.pl (J. Chróścielewski), eremeyev.victor@gmail.com (V.A. Eremeyev).

some critical aspects of this problem which we have experienced during numerous nonlinear finite element analyses of structures and to draw attention to some basic difficulties which are not dealt with in the majority of numerically oriented papers in this field.

As an example we consider an "elementary" problem of finding equilibrium paths for a circular arch simply supported at both ends and loaded by a concentrated force at the apex. An example like that can be found in almost every paper on nonlinear finite element analysis of structures, see e.g. Boutyour, Zahrouni, Potier-Ferry, and Boudi (2004), Killpack and Abed-Meraim (2011), Leahu-Aluas and Abed-Meraim (2011), Simo and Vu-Quoc (1986), Simo, Wriggers, Schweizerhof, and Taylor (1986), Turco, Barchiesi, Giorgio, and DellIsola (2020), Waszczyszyn (1983) and Wriggers and Simo (1990). Moreover, the interest to arches in civil engineering is still continued due to interesting and complex behaviour, see e.g. recent papers by Champneys et al. (2019), Hu, Li, and Hu (2021), Hu, Pi, Gao, and Li (2018), Li and Zheng (2019), Pi, Bradford, and Guo (2016) and Wriggers (2017). If the arch is very shallow the load–deflection path is rather simple and can be found without any essential difficulties. For increasing span to rise ratio the solutions become more and more complex exhibiting the so-called loops of the load–deflection curve during the symmetric snap-through. In addition, non-symmetric solutions bifurcate from the primary equilibrium path and secondary or even higher order bifurcation points may appear. In these cases tracing of the load deflection curves becomes a quite involved task which requires effective path-following methods for solutions of the nonlinear operator equations enabling one to detect singular (limit or bifurcation) points. As the buckled arches are capable to carry loads in the postbuckling range, the analysis of postbifurcation deformations constitutes not only a mathematical problem but an engineering one. Let us note that here we have highly nonlinear regimes of deformations, which relate to large translations and rotations. This may result in looping of equilibrium paths (deformation curves). In the case of non-shallow arches here we faced both geometrical and structural nonlinearities that brings this complexity in solution.

This problem has received much attention in the mathematical as well as engineering literature, so e.g. in the work by Wriggers and Simo (1990), who deal with the formulation and numerical implementation of general purpose algorithms for the direct computation of stability points within the context of finite element formulations in non-linear solid mechanics. However, in spite of these interesting developments there are certain phenomena connected with the nonlinear behaviour in general and with the use of the Finite Element Method in particular, which have not yet been solved sufficiently and which will be addressed in this paper. We shall demonstrate this by comparing our results with those presented in Wriggers and Simo (1990) and examine in this context more closely some difficulties lying behind the solution of such a nonlinear structural problem in general.

We shall show, in particular, that symmetric solutions characterized by typical loops of the load deflection curve may change completely (not only quantitatively, but also qualitatively) with a refinement of the finite element mesh as well as with the use of different theories which lead to different types (e.g. C^0, C^1) of elements. For the arch problem under consideration we present solutions for different discretizations which clearly show that with the exception of initial and final loops all remaining parts of the load deflection curve during the symmetric snap through are most often questionable, because the wavelength of the deformation pattern becomes extremely small for higher order loops. The problem of reliability of finite element approximations increases dramatically with decreasing wavelength of the deformation pattern, which is typical not only for snap-through loops, but also for problems involving high frequency vibrations and propagation of short waves.

In addition, we shall present non-symmetric solutions for the arch problem under consideration including also bifurcation points and equilibrium paths which have not yet been reported in literature. These solutions allow for the correct interpretation of certain points in the load–deflection paths which have not been recognized as bifurcation points in earlier literature. In particular we shall also present a bifurcation point in a secondary, already bifurcated path, leading to a tertiary equilibrium path. To the best of our knowledge such a phenomenon has not yet been presented in nonlinear analysis of structures at all.

However, the provided analysis shows that one has to be aware of the fact that the complete solution can be obtained in this way. The long term experience of the first author suggests that the attempt to obtain the complete and correct finite element solution for nonlinear structural problems like the one considered here is a rather hopeless task (hence the title of this work).

2. Shear-deformable beam model

2.1. Governing equations

Let us consider a planar deformation of a naturally curved plane elastic rod. We take the (x, y)-plane spanned by the orthonormal basis $\{\mathbf{e}_1, \mathbf{e}_2\}$ to be the plane of the rod deformation. Our subsequent analysis is based on Reissner's theory of plane deformation of rods which is rich enough to accommodate the longitudinal extension, flexure and shear (Reissner, 1972). In this theory a deformation of the rod is completely determined by two Cartesian components (u, w) of the displacement of the rod axis and a mean rotation ψ of the cross-section which we write collectively as the vector $\mathbf{u}(\xi) = \{u(\xi), w(\xi), \psi(\xi)\}^T$. Here $\xi \in [a, b]$ denotes an arbitrary arc-length parameter along the undeformed rod axis. The associated strains constitute the vector $\boldsymbol{\varepsilon}(\xi) = \{\varepsilon(\xi), \gamma(\xi), \kappa(\xi)\}^T$ consisting of the stretching strain, the shear strain and the bending strain, respectively. The strain–displacement relations take the form

$$\boldsymbol{\varepsilon}(\xi) = \begin{Bmatrix} \varepsilon(\xi) \\ \gamma(\xi) \\ \kappa(\xi) \end{Bmatrix} = \begin{Bmatrix} \alpha_{\xi}^{-1}(C u_{,\xi} + S w_{,\xi}) + \cos\psi - 1 \\ \alpha_{\xi}^{-1}(-S u_{,\xi} + C w_{,\xi}) + \sin\psi \\ \alpha_{\xi}^{-1}\psi_{,\xi} \end{Bmatrix}, \tag{1}$$

where α_{ξ} denotes the Lamé coefficient, so $ds \equiv \alpha_{\xi}d\xi$ is an elementary length, $S(\xi) \equiv \sin(\phi - \psi)$ and $C(\xi) \equiv \cos(\phi - \psi)$. Here ϕ denotes the angle between x-axis and the tangent to the undeformed rod axis. The work-conjugate stress measures constitute the

triple $\mathbf{S}(\xi) = \{N(\xi), Q(\xi), M(\xi)\}^T$ consisting of the normal stress resultant N, the shear stress resultant Q and the couple M. The principle of virtual work expressing equilibrium conditions takes the form

$$G[\mathbf{u}; \delta\mathbf{u}] \equiv \int \delta\boldsymbol{\varepsilon}^T \mathbf{S}\alpha_\xi \mathrm{d}\xi - \delta W = \int (N\delta\varepsilon + Q\delta\gamma + M\delta\kappa)\alpha_\xi \mathrm{d}\xi - \delta W = 0, \tag{2}$$

for every kinematically admissible virtual displacement $\delta\mathbf{u}$. Here δW stands for the virtual work of the external loads which must be specified for each type of loads. For a thin linear elastic rod the stress–strain relations take classical form

$$N = EF\varepsilon, \quad Q = k_s GF\gamma, \quad M = EI\kappa, \tag{3}$$

where E and G denote the Young and shear moduli, F area of the rod cross-section, I moment of inertia, and k_s shear correction factor, respectively.

From (2) and applying standard variational procedure the complete set of field equations and boundary conditions can easily be derived. It is essential to the subsequent analysis that this rod theory is geometrically exact in the sense that neither displacements nor rotation are limited in whatever magnitude.

2.2. Lagrange family of finite elements

An attractive feature of this theory is that only C^0-continuity of $\mathbf{u}$ is required. Thus, following the standard finite element procedure the rod is discretized into a finite number of n-node elements. Within an isoparametric concept the typical element is defined as a smooth image of the standard element $\pi_e = [-1, +1]$, and the displacements are interpolated according to

$$\mathbf{u}(\xi) = \begin{Bmatrix} u(\xi) \\ w(\xi) \\ \psi(\xi) \end{Bmatrix} = \sum_{a=1}^n L_a(\xi) \begin{Bmatrix} u_a \\ w_a \\ \psi_a \end{Bmatrix} \equiv \sum_{a=1}^n L_a(\xi)\mathbf{u}_a, \quad \mathbf{u}_a = \begin{Bmatrix} u_a \\ w_a \\ \psi_a \end{Bmatrix} \tag{4}$$

where $\xi \in [-1, 1]$ now denotes the natural coordinate and $L_a(\xi)$ are the Lagrange shape functions which for the n-node element are given by

$$L_a(\xi) = \prod_{\substack{a,b=1 \\ a \neq b}}^n \frac{\xi - \xi_a}{\xi_a - \xi_b}, \quad a, b = 1, 2, \ldots, n. \tag{5}$$

It is a basic concept of the isoparametric finite elements that the initial geometry of the rod is interpolated using the same scheme (5). Substituting the interpolation (5) into the principle of virtual work (2) and following the standard finite elements procedure one gets

$$G[\mathbf{q}; \delta\mathbf{q}] \equiv \delta\mathbf{q}^T \mathbf{f}(\mathbf{q}) = 0. \tag{6}$$

Here $\mathbf{q}$ denotes the global vector of nodal displacements and $\mathbf{f}(\mathbf{q}) = \mathbf{0}$ is the discrete form of the equilibrium equations. The element matrices resulting from the consistent linearization of (2) or equivalently (6) can next be calculated in the standard way. The results presented in the following were obtained using 2-, 3-, and 4-node elements. To avoid locking effects using 2- and 3-node elements the reduced integration (RI) was applied with 1 and 2 sampling points, respectively. As 4-node element practically does not exhibit locking, the full 4-points integration procedure (FI) was utilized. Let us note that used here C^0 beam elements were developed as a collateral result of the finite element modelling within six-parameter theory of shells in Chróścielewski, dellIsola, Eremeyev, and Sabik (2020), Chróścielewski, Makowski, and Pietraszkiewicz (2004), Chróścielewski, Sabik et al. (2019) and Daszkiewicz, Witkowski, Burzyński, and Chróścielewski (2019). In fact, beam elements could be treated as a reduction of two-dimensional shell elements to one dimension. In particular, this was mentioned in the last section by Chróścielewski, Makowski, and Stumpf (1992).

3. Non shear-deformable beam

3.1. Governing equations

Our ultimate goal is to expose the complexity of highly nonlinear problems and of the related problem of the accuracy of finite element approximations. To gain deeper insight into this we shall carry out parallel analysis based on the beam theory in which the shear strain is constrained to vanish $\gamma = 0$. By implication the mean rotation ψ is no longer independent variables but it can be expressed in terms of the displacements of the beam axis. In this case it is more convenient to resolve the displacement vector of the beam axis into the tangential u_t and normal u_n components relative to the undeformed axis. As before we set $\mathbf{u} = \{u_t, u_n\}^T$ and $\boldsymbol{\varepsilon} = \{\varepsilon, \kappa\}^T$ with the strains ε and κ previously defined and subjected to the constraint $\gamma = 0$. Then the strain–displacement relations take the form

$$\boldsymbol{\varepsilon}(\xi) = \begin{Bmatrix} \varepsilon(\xi) \\ \kappa(\xi) \end{Bmatrix} = \begin{Bmatrix} \lambda - 1 \\ \alpha_\xi^{-1}\lambda^{-2}\left[-\varphi_{,\xi}(1+\vartheta) + \varphi\vartheta_{,\xi}\right] \end{Bmatrix}, \tag{7}$$

where

$$\lambda(\xi) = \sqrt{(1+\vartheta)^2 + \varphi^2} \tag{8}$$

denotes the stretch along the beam axis and φ and ϑ are linearized parameters defined in terms of displacements by

$$\vartheta(\xi) = \alpha_\xi^{-1} u_{t,\xi} - K u_n, \quad \varphi(\xi) = \alpha_\xi^{-1} u_{n,\xi} + K u_t \tag{9}$$

Here $K = \alpha_\xi^{-1} \phi_{,\xi}$ is the curvature of the undeformed beam axis. The work-conjugate stress measures are $\mathbf{S} = \{N, M\}^T$ and the equilibrium conditions are again expressed in the form of the principle of virtual work

$$G[\mathbf{u}; \delta\mathbf{u}] \equiv \int \delta\varepsilon^T \mathbf{S} \, \alpha_\xi \mathrm{d}\,\xi - \delta W = \int (N\delta\varepsilon + M\delta\kappa)\alpha_\xi \mathrm{d}\,\xi - \delta W = 0. \tag{10}$$

The stress–strain relations take now the same form for N and M

$$N = EF\varepsilon, \quad M = EI\kappa, \tag{11}$$

whereas Q plays the role of a Lagrange multiplier for constraint $\gamma = 0$ and should be determined from the equilibrium equations. In (11) E, F and I have the meaning previously defined in (3). The derivation of the resulting field equations and boundary conditions follows then in a classical way. It is only essential to point it out that like in the case of shear-deformable beam model there are nor restrictions whatsoever as the magnitude of the displacements and rotation concerns.

3.2. Finite element discretization

From the numerical point of view, the non-shear-deformable beam model has this distinguishing feature that it requires C^1-interelement continuity (Hermitian interpolation) to obtain a conforming finite element method. To ensure this continuity requirement we consider the two-node element with four degrees of freedom at each node resulting in the interpolation scheme

$$\mathbf{u}(\xi) = \begin{Bmatrix} u_t(\xi) \\ u_n(\xi) \end{Bmatrix} = \sum_{a=1}^{2} \mathsf{H}_a(\xi)\mathbf{u}_a, \tag{12}$$

$$\mathsf{H}_a(\xi) = \begin{bmatrix} H_a(\xi) & \alpha_\xi H_a'(\xi) & 0 & 0 \\ 0 & 0 & H_a(\xi) & \alpha_\xi H_a'(\xi) \end{bmatrix}, \quad \mathbf{u}_a = \begin{Bmatrix} u_{ta} \\ u_{ta}' \\ u_{na} \\ u_{na}' \end{Bmatrix}$$

where $\xi \in [-1, 1]$ denotes the natural coordinate and $H_a(\xi)$ and $H_a'(\xi)$ are the Hermitian shape functions which for the two node element are given by

$$H_1(\xi) = 1 - 3\xi^2 + 2\xi^3, \quad H_1'(\xi) = \xi - 2\xi^2 + \xi^3,$$

$$H_2(\xi) = 3\xi^2 - 2\xi^3, \quad H_2'(\xi) = -\xi^2 + \xi^3.$$

Here a prime $(\cdot)'$ stands for the derivative with respect to the arc length parameter along the undeformed rod axis so that u_t' and u_n' are dimensionless quantities. Substituting the interpolation (12) into the principle of virtual work (10) and following again the standard finite elements procedure one gets

$$G[\mathbf{q}; \delta\mathbf{q}] \equiv \delta\mathbf{q}^T \mathbf{f}(\mathbf{q}) = 0. \tag{13}$$

Here $\mathbf{q}$ denotes the global vector of nodal degrees of freedom and $\mathbf{f}(\mathbf{q}) = 0$ is the discrete form of the equilibrium conditions. In contrast to the finite element approximation, within the element we represent exactly the initial geometry of the beam. Moreover, this element does not exhibit the locking effects and no reduced integration is needed. Thus, in evaluation of element matrices we apply the Gauss–Legendre numerical integration with three sampling points.

As in the case of C^0 beam elements, C^1 beam finite elements can be treated as 2D-to $-$1D reductions of shell elements developed for Kirchhoff–Love shells, see e.g. Makowski and Stumpf (1986), Nolte, Makowski, and Stumpf (1986) and Stumpf and Makowski (1987) and their numerical implementation discussed in Chróścielewski and Nolte (1985) and Nolte and Chróścielewski (1986).

4. Numerical analysis of a simply supported circular arch

The problem to be examined in the sequel consists of the circular arch simply supported at both ends and loaded by a downward concentrated force applied at the apex. The geometry and material date, being exactly those assumed by Wriggers and Simo (1990), are shown in Fig. 1. Hereinafter the following values of parameters were used: $EA = GA = EI = 10^6$, $R = 100$, $\alpha = 210°$. Other types of boundary conditions could be studied in a similar way as well as other geometrical parameters. For example, in the case of linear analysis some results on critical force as a function of the span can be found in Bažant and Cedolin (2010) and Timoshenko and Gere (1963). Let us note that in the case of a clamped–clamped arch we have less complex behaviour of the load–deflection curves as in this case the structure becomes more stiff, in general. So in the following we consider a most complex case of non-shallow flexible arch.

The solutions presented in the following were obtained using the finite element method shortly described in Sections 2 and 3. We present the solutions for four different discretizations denoted by 20e2, 20e4, 36e4, 72e4, etc., for the C^0 element type, and
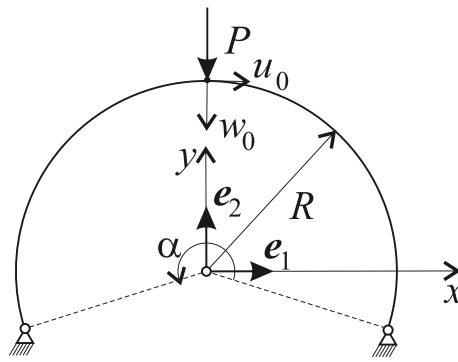
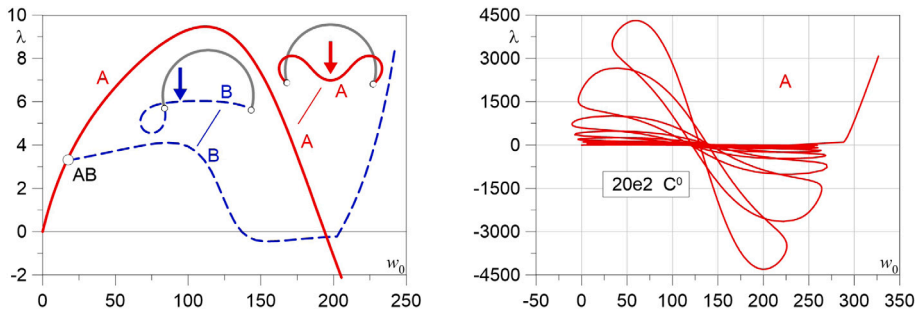**Fig. 1.** Circular arch under point load at the apex.

Fig. 2. Load–deflection curves, the first A and secondary B paths (on the left); load–deflection curve, the first path (on the right). After Wriggers and Simo (1990).

20e2, 160e2 for the C^1 element type, respectively. The meaning of these designations is the following: the first number denotes the assumed number of elements, the second one stands for the number of nodes per element. For example, 20e4 denotes the discretization of the arch into twenty 4-node elements.

It should be emphasized that the discussed highly nonlinear problems require effective control methods. The algorithm developed by us takes into account three ways of control, that are control of loads, displacements and arc length, respectively. We use, among others, to overcome the problem with different units and orders of magnitudes of coordinate vectors, the technique of selective elimination or scaling of the arc-length and norms for convergence control, which were first proposed by Chróścielewski and Nolte (1985); and the control window technique was presented by Chróścielewski and Schmidt (1985). A current description of the algorithm can be found in Chróścielewski, Schmidt et al. (2019) among others.

For comparison we adopted the discretization 20e2 C^0-elements which was used in Simo, Hjelmstad, and Taylor (1984) and Wriggers and Simo (1990). In the presentation of results we shall show the displacements in Fig. 2.

Let us note that on the postbifurcation path B there is another bifurcation point. As a result, path B given by Wriggers and Simo (1990) consists of two paths B and C, see Figs. 13–15 for comparison. The latter gives a solution in the case of symmetric deformations. This was discussed earlier by Chróścielewski and Lubowiecka (2001).

4.1. Symmetric solutions using C^0 elements

Figs. 3–4 show the load–deflection curve for the apex and Figs. 5–7 for the rotation angle at a support. These curves are related to symmetric deformations (i.e. to the primary equilibrium path A) of the arch and show typical loops during a snap-through. The solution for the apex deflection obtained with the 20e2 discretization is exactly the same as the one given by Wriggers and Simo (1990). Here it is compared with solutions obtained by 20e4, 36e4 and 72e4 discretizations. One observes large qualitative and quantitative differences with an increasing number of degrees of freedom and/or elements. It is seen that the form and the number of loops change considerably with the mesh refinement. Large quantitative differences can be observed especially in the graphs for the rotation angle at a support, the range of which decreases drastically with increasing number of elements.

Fig. 8 shows some arch configurations in different loops of the load–deflection curve obtained with the 72e4 C^0-elements discretization. In Fig. 9 the left half of several deformed configurations are presented, which the arch assumes during various loops passing upwards or downwards through the line connecting the supports. Here it is seen that during the snap-through the wave length of the deformation pattern becomes very small. As long as the element length is not small enough to model such a deformation pattern, one cannot expect correct results. Since the birth of each wave in the deformation pattern is reflected as a loop in the
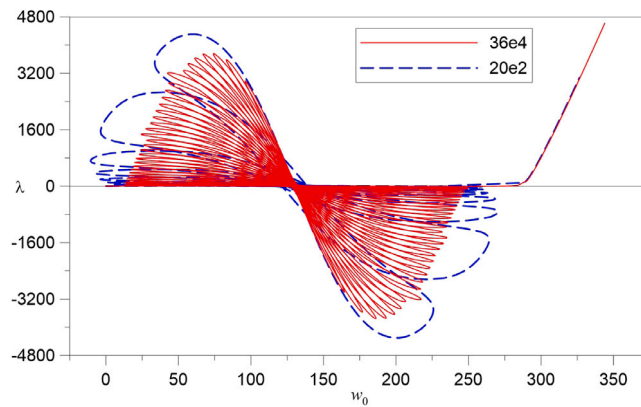
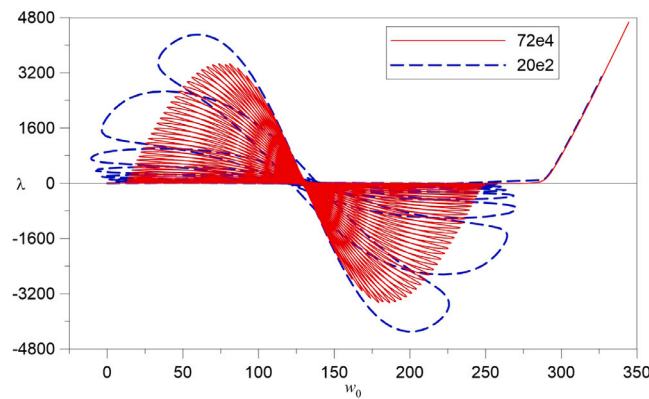**Fig. 3.** Deflection w_0 *vs.* load λ calculated with 20 2-node (20e2) and 36 4-node (36e4) C^0-finite elements.

Fig. 4. Deflection w_0 *vs.* load λ calculated with 20 2-node (20e2) and 74 4-node (74e4) C^0-finite elements.
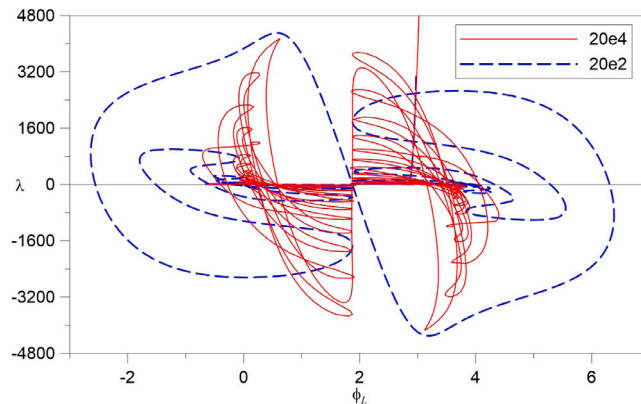

Fig. 5. The rotation angle at the left support ϕ_L *vs.* load λ calculated with 20 2- and 4-node C^0-finite elements, (20e2 and 20e4 schemes).

load–deflection curve, it is understandable that results obtained by a poor discretization show less loops. In view of these results it should be emphasized that the different number of loops for different number of elements and/or degrees of freedom is only a result of the finite element approximation. Hence, for problems whose load–deflection curve exhibits such loops the question arises, how many elements and/or degrees of freedom are necessary to model the physical phenomenon properly. Furthermore, it can be observed that the number of such loops increases e.g. with increasing span to rise ratio. Therefore, independently of the solution method applied the additional question arises, if the number of loops is finite for generalized arch data (geometrical, material, etc.) and if it is possible at all to obtain the complete and fully correct solution by discrete methods.
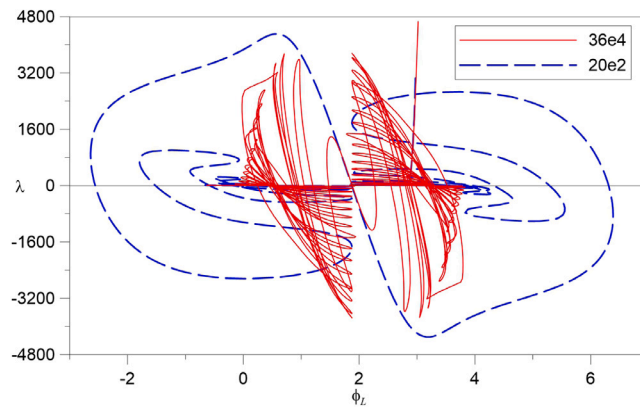
Fig. 6. The rotation angle at the left support ϕ_L *vs.* load λ calculated with 20 2-node (20e2) and 36 4-node (36e4) C^0-finite elements.
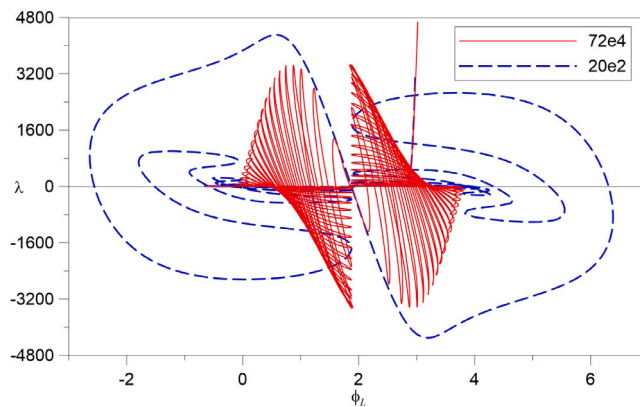

Fig. 7. The rotation angle at the left support ϕ_L *vs.* load λ calculated with 20 2-node (20e2) and 72 4-node (72e4) C^0-finite elements.
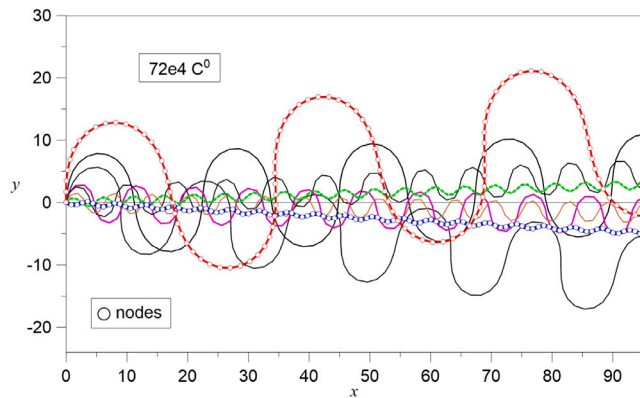

Fig. 8. Selected arch configurations in the vicinity of buckling, calculated with 72e4 C^0 elements.

4.2. Symmetric solutions using C^1 elements

In view of the problems which we have encountered in the preceding section during the analysis of the arch using C^0-elements, we now check the possibilities of a higher-order element with C^1-continuity presented in Section 3. Since this element is based on the Bernoulli hypothesis, it does not take into account transverse shear deformations. The arch under consideration is so flexible that shear deformations should not play any role, as long as the wavelength of the deformation pattern is sufficiently large. For the primary equilibrium path it can be expected that this is the case during the initial and final snap-through loops. Hence, for these regions of the load–deflection curve we can expect that in a comparative finite element analysis with C^0- and C^1-elements we really
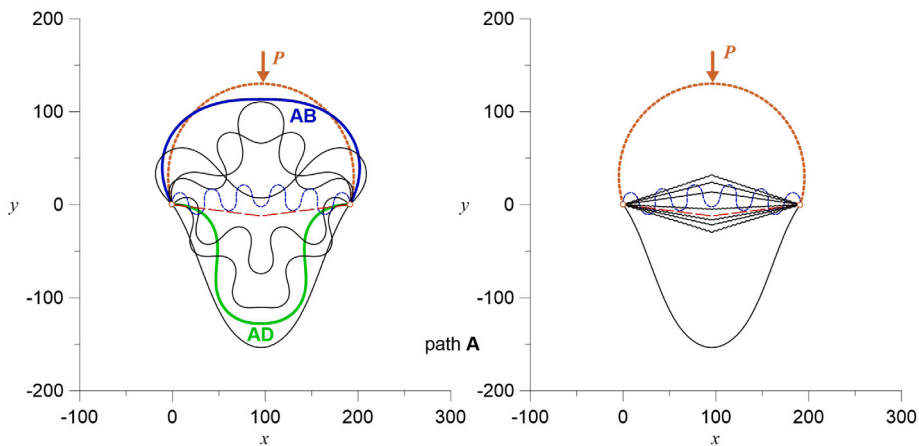
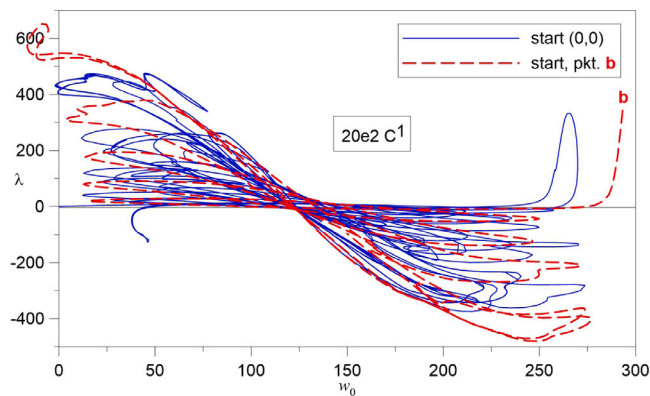**Fig. 9.** Selected arch configurations calculated with 72e4 C^0 elements.

Fig. 10. Deflection w_0 *vs.* load λ calculated with 20 2-node C^1-finite elements.
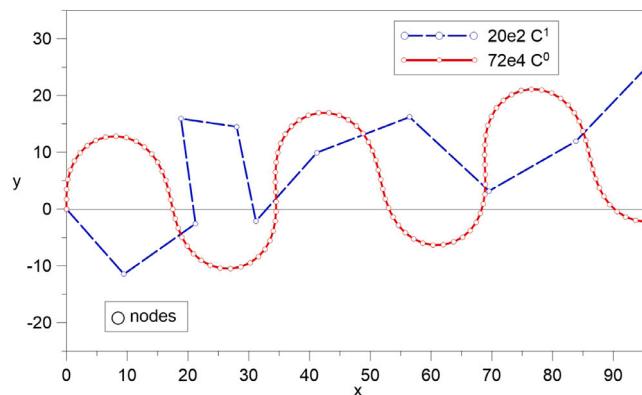

Fig. 11. Arch configurations in the vicinity of buckling, calculated with 20e2 C^1 and 72e4 C^0 elements.

compare these two types of elements and not the underlying theories (i.e. shear-deformable beams and Bernoulli beams theories, respectively).

Fig. 10 shows results for the centre deflection obtained with a discretization of 20e2 C^1-elements. If these are compared to the C^0-element solutions, we observe large qualitative differences as far as higher-order loops are concerned, which assume a completely irregular shape of equilibrium shapes as well as deformations, as shown in Fig. 11. Such irregular forms disappear if the finite element mesh is refined, as can be seen in Fig. 12, where 160e2 C^1-elements have been used. In contrast to Fig. 10 we have observed here
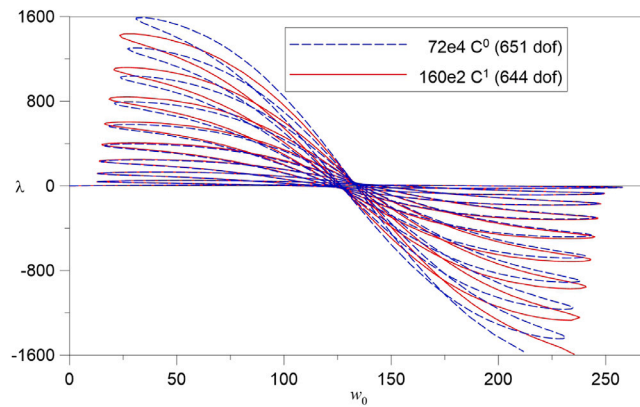
Fig. 12. Deflection w_0 *vs.* load λ calculated with 160e2-node C^1 and 74e4 C^0-finite elements. Begin of calculations.
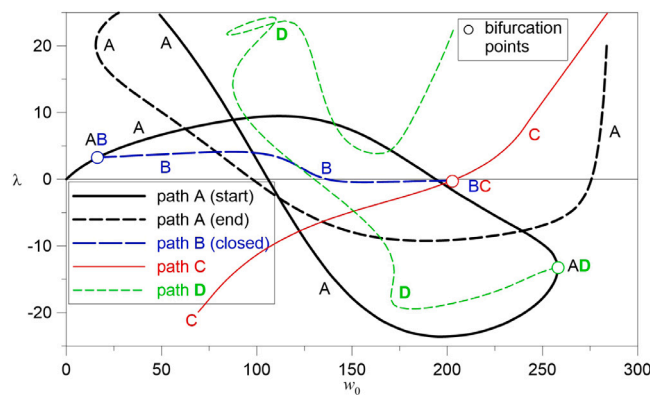

Fig. 13. Load–deflection curves, various paths, calculated with 160 2-node C^1-finite elements.

also completely regular deformation patterns. This shows that the arch discretization has lost the capability to model the deformed arch, because the wavelength is already too short. Apparently C^1-continuity is not so flexible in discretizations as C^0-continuity is.

In Fig. 12 we have compared the initial parts of the load–deflection curves obtained with 160e2 C^1- and 72e4 C^0-element discretizations (which have approximately the same number of degrees of freedom) up to such loops where significant quantitative differences can be observed. At the beginning there is a very good agreement between these two solutions. Increasing differences can be observed during the development of the deformation process where the C^0-element solution predicts a softer response. Here the question arises, if this is already an effect of decreasing wavelength of the deformation pattern where the effect of shear deformation becomes significant, or just a result of different finite element approximations.

4.3. Secondary symmetric and nonsymmetric solutions

For the analysis of the arch deformations we are also interested in secondary solutions presented in Figs. 13–17. In order to limit our discussion on influence of discretization on the results, we restrict ourselves to the 160 2-node C^1-finite elements. Fig. 13 shows deflection w_0 vs. load λ, whereas horizontal displacement u_0 at the apex is given in Fig. 14. Rotation angles at the arch ends are presented in Fig. 15. Selected arch static configurations for secondary paths are given in Figs. 16 and 17. What is interesting here is that there exist next the bifurcation point AD on the primary path A and related postbifurcation path D, that was not known in the literature, see Fig. 17 for corresponding equilibrium shapes. Let us underline that in the case of arches their height (or the angle for circular arches) plays an essential role. Indeed, for deep arches one can expect nonsymmetric buckling first even in the case of symmetric geometry and boundary conditions. This make the picture of postbifurcation deformations much more complex as we can see in these figures.

Conclusions

We discussed postcritical behaviour of a shear deformable and non-shear deformable circular non-shallow arch using various types of finite elements and various approximations. Summarizing one can say that like in the analysis of the arch using C^0 and C^1-elements and also here during the developing deformation process the solution changes qualitatively with increasing number of C^0
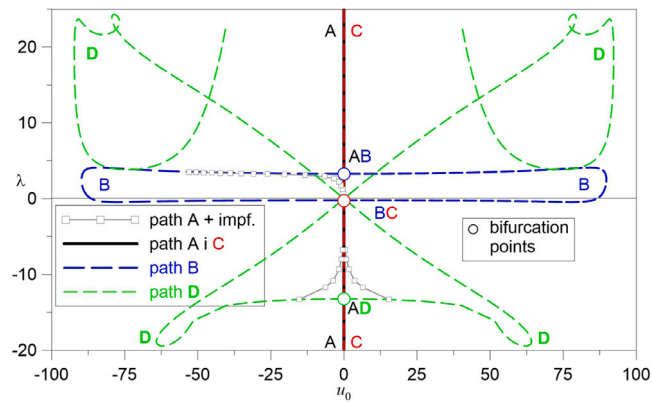
Fig. 14. The horizontal displacement u_0 in the arch apex calculated with 160 2-node C^1-finite elements.
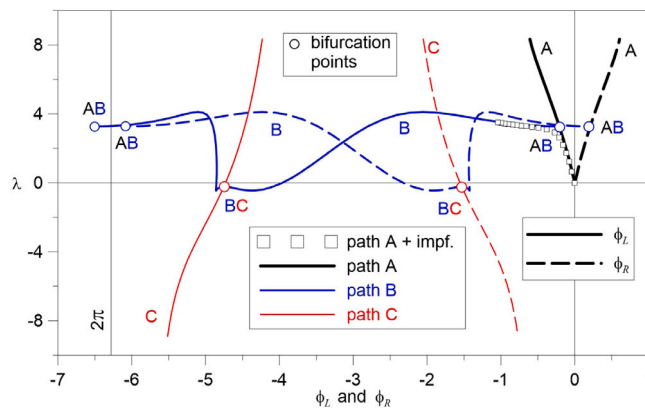

Fig. 15. The rotation angles at the arch ends calculated with 160 2-node C^1-finite elements.
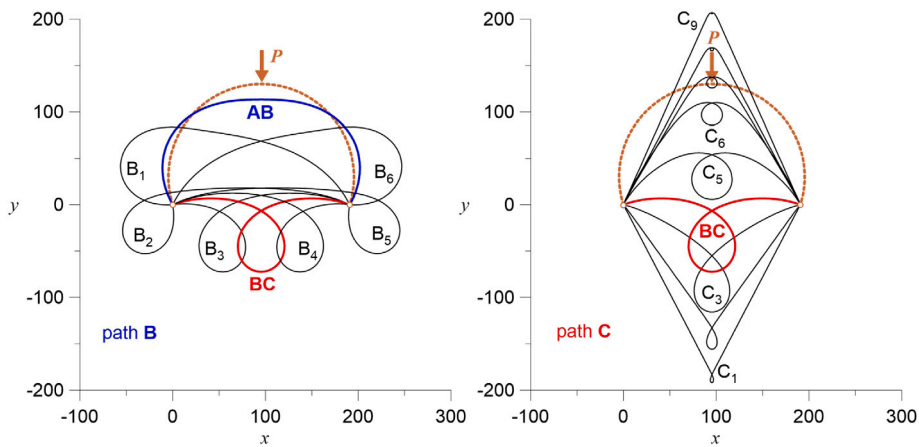

Fig. 16. Selected arch configurations calculated with 160 2-node C^1-finite elements, paths B and C.

and C^1-elements. This shows that for both types of elements the obtained solutions only in limited parts of the range of deformation are rational. On the basis of such comparative numerical investigations in literature often conclusions are drawn concerning the validity, accuracy, performance, and other characteristics of theories and algorithms. In the light of the results presented here this should be done with great carefulness, because it may lead easily to wrong conclusions. In particular, considering a relatively simple problem we found another equilibrium path D previously unknown.
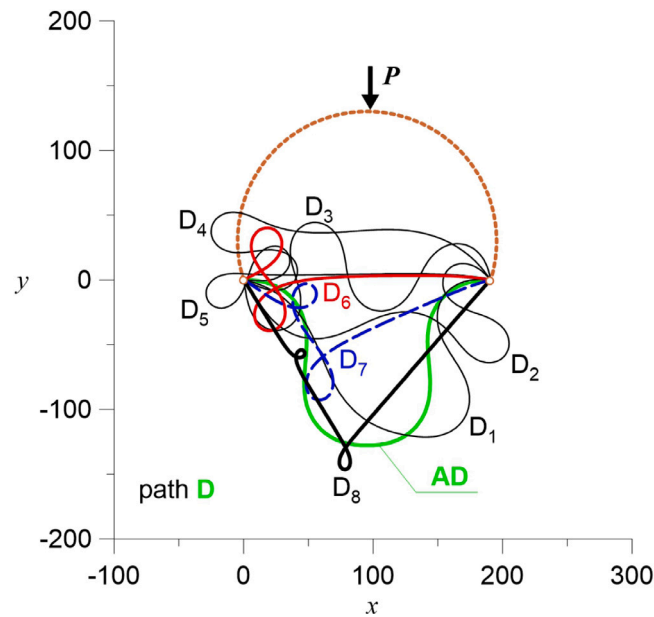
Fig. 17. Selected arch configurations calculated with 160 2-node C^1-finite elements, path D.

Let us also note that FEM represents discrete models, so a correspondence between FEM model and its continuum counterpart may be generalized up to the level of correspondence between discrete and continuum models of mechanics in the case of buckling analysis. Well-posed continuum models have countable spectrum, i.e. bifurcations are countable, whereas by definition discrete models possess only a finite number of eigen-modes. It means that any discrete model cannot describe the whole spectrum of the continuum model, but usually this is not necessary. For example, von Mises truss introduced one hundred years ago (Mises, 1923) can be interpreted as a finite discretization of an arch using only two elements. Nevertheless, it demonstrates rather complex behaviour including symmetric and non-symmetric buckling, snap-through and snap-back behaviour (Feodosiev, 2005; Perelmuter & Slivker, 2013; Pignataro, Rizzi, & Luongo, 1991), especially for trusses with large height. Obviously, it cannot describe all possible solutions for the arch but at least some initial bifurcations could be predicted.

It is also well-known that arches and shells are very sensitive to imperfections. As any discretization provides some imperfections in comparison with the continuum model, this also may result in difficulties in convergence of the discrete solution to the continuum one. It could be even impossible without proper analysis as in the case of the polygon-circle paradox (Babuška & Pitkäranta, 1990; Simmonds, 2010). Similar sensitivity of critical loads also relates to boundary conditions. For example, for other types of boundary conditions we will have different behaviour after bifurcation, in general.

On the other hand, considering lattice dynamics (Born & Huang, 1985; Ostoja-Starzewski, 2002) we can see that it brings more than some continuum limits. Moreover, for a discrete model one can propose various continuum limits. For example, considering discrete and continuum models of elastica discussed by Challamel, Kocsis, and Wang (2015), Kocsis and Challamel (2016) and Zhang, Challamel, Wang, and Zhang (2019), it was shown that extended continuum model can give only a part of bifurcation behaviour. So the title question can be transformed not only into "Discrete is it enough?" as in Turco (2018) or into "Continuum is it enough?". Answers for both questions constitute a rather interesting topic for future investigations.

Declaration of competing interest

The authors declare that they have no known competing financial interests or personal relationships that could have appeared to influence the work reported in this paper.

Data availability

Data will be made available on request.

Acknowledgments

References

Amabili, M. (2008). *Nonlinear vibrations and stability of shells and plates*. Cambridge: Cambridge University Press.

Antman, S. S. (2005). *Nonlinear problems of elasticity* (2nd ed.). New York: Springer.

Babuška, I., & Pitkäranta, J. (1990). The plate paradox for hard and soft simple support. *SIAM Journal on Mathematical Analysis, 21*, 551–576.

Barretta, R., Čanadija, M., Luciano, R., & de Sciarra, F. M. (2022). On the mechanics of nanobeams on nano-foundations. *International Journal of Engineering Science, 180*, Article 103747.

Bažant, Z. P., & Cedolin, L. (1990). *Stability of structures*. Oxford: Oxford University Press.

Bažant, Z. P., & Cedolin, L. (2010). *Stability of structures. elastic, inelastic, fracture and damage theories*. World Scientific Publishing.

Born, M., & Huang, K. (1985). *The international series of monographs on physics. Oxford classic texts in the physical sciences, Dynamical theory of crystal lattices*. Oxford: The Clarendon Press, Oxford University Press.

Boutyour, E. H., Zahrouni, H., Potier-Ferry, M., & Boudi, M. (2004). Bifurcation points and bifurcated branches by an asymptotic numerical method and Padé approximants. *International Journal for Numerical Methods in Engineering, 60*, 1987–2012.

Challamel, N., Kocsis, A., & Wang, C. (2015). Discrete and non-local elastica. *International Journal of Non-Linear Mechanics, 77*, 128–140.

Champneys, A. R., Dodwell, T. J., Groh, R. M., Hunt, G. W., Neville, R. M., Pirrera, A., Sakhaei, A. H., Schenk, M., & Wadee, M. A. (2019). Happy catastrophe: recent progress in analysis and exploitation of elastic instability. *Frontiers in Applied Mathematics and Statistics, 5*(34).

Chen, W., Wang, L., & Yan, Z. (2023). On the dynamics of curved magnetoactive soft beams. *International Journal of Engineering Science, 183*, Article 103792.

Choudhury, P. K. (Ed.), (2022). *Metamaterials: technology and applications*. Boca Raton: CRC Press.

Chróścielewski, J., dellIsola, F., Eremeyev, V. A., & Sabik, A. (2020). On rotational instability within the nonlinear six-parameter shell theory. *International Journal of Solids and Structures, 196*, 179–189.

Chróścielewski, J., & Lubowiecka, I. (2001). On convergence of solution of nonlinear fem considering an arch (in Polish). In *VI konferencja naukowo-techniczna programy MES W komputerowym wspomaganiu analizy, projektowania i wytwarzania* (pp. 21–29). Warszawa–Rynia: Wojskowa Akademia Techniczna, Wydział Mechaniczny, Instytut Materiałoznawstwa i Mechaniki Technicznej.

Chróścielewski, J., Makowski, J., & Pietraszkiewicz, W. (2004). *Statics and dynamics of multyfolded shells. Nonlinear theory and finite element method (in Polish)*. Warszawa: Wydawnictwo IPPT PAN.

Chróścielewski, J., Makowski, J., & Stumpf, H. (1992). Genuinely resultant shell finite elements accounting for geometric and material non-linearity. *International Journal for Numerical Methods in Engineering, 35*, 63–94.

Chróścielewski, J., & Nolte, L.-P. (1985). *Mitt. institut für mechanik: Vol. 48, Strategien zur lösung nichtlinearer probleme der strukturmechanik und ihre modulare aufbereitung im konzept MESY (in German) volume 48*. Bochum: Ruhr-Universität Bochum.

Chróścielewski, J., Sabik, A., Sobczyk, B., & Witkowski, W. (2019). 2-D constitutive equations for orthotropic cosserat type laminated shells in finite element analysis. *Composites Part B (Engineering), 165*, 335–353.

Chróścielewski, J., & Schmidt, R. (1985). A solution control method for nonlinear finite element post-buckling analysis of structures. In J. Szabó (Ed.), *Post-buckling of elastic structures. Proc. of the EUROMECH - colloquium nr. 200, màtrafüred (Hungary)* (pp. 19–33). Amsterdam: Elsevier.

Chróścielewski, J., Schmidt, R., & Eremeyev, V. A. (2019). Nonlinear finite element modeling of vibration control of plane rod-type structural members with integrated piezoelectric patches. *Continuum Mechanics and Thermodynamics, 31*, 147–188.

Civalek, Ö., Uzun, B., & Yaylı, M. Ö. (2023). On nonlinear stability analysis of saturated embedded porous nanobeams. *International Journal of Engineering Science, 190*, Article 103898.

Darban, H., Luciano, R., Caporale, A., & Fabbrocino, F. (2020). Higher modes of buckling in shear deformable nanobeams. *International Journal of Engineering Science, 154*, Article 103338.

Dastjerdi, S., Alibakhshi, A., Akgöz, B., & Civalek, Ö. (2023). On a comprehensive analysis for mechanical problems of spherical structures. *International Journal of Engineering Science, 183*, Article 103796.

Daszkiewicz, K., Witkowski, W., Burzyński, S., & Chróścielewski, J. (2019). Robust four-node elements based on Hu–Washizu principle for nonlinear analysis of cosserat shells. *Continuum Mechanics and Thermodynamics, 31*, 1757–1784.

Dehrouyeh-Semnani, A. M. (2021). On large deformation and stability of microcantilevers under follower load. *International Journal of Engineering Science, 168*, Article 103549.

dell'Isola, F., & Steigmann, D. J. (2020). *Discrete and continuum models for complex metamaterials*. Cambridge: Cambridge University Press.

Epstein, M., & Javadi, M. (2023). Kinematically exact formulation of large deformations of gradient elastic beams. *International Journal of Engineering Science, 186*, Article 103827.

Feodosiev, V. I. (2005). *Advanced stress and stability analysis: worked examples*. Berlin: Springer.

Gholipour, A., & Ghayesh, M. H. (2020). Nonlinear coupled mechanics of functionally graded nanobeams. *International Journal of Engineering Science, 150*, Article 103221.

Hu, C.-F., Li, Z., & Hu, Q.-S. (2021). On non-linear behavior and buckling of arch-beam structures. *Engineering Structures, 239*, Article 112214.

Hu, C.-F., Pi, Y.-L., Gao, W., & Li, L. (2018). In-plane non-linear elastic stability of parabolic arches with different rise-to-span ratios. *Thin-Walled Structures, 129*, 74–84.

Kapitaniak, M., Vaziri, V., & Wiercigroch, M. (2020). Bifurcation scenarios in helical buckling of slender rods using new FE. *International Journal of Engineering Science, 147*, Article 103197.

Khaniki, H. B., & Ghayesh, M. H. (2023). Highly nonlinear hyperelastic shells: Statics and dynamics. *International Journal of Engineering Science, 183*, Article 103794.

Killpack, M., & Abed-Meraim, F. (2011). Limit-point buckling analyses using solid, shell and solid-shell elements. *Journal of Mechanical Science and Technology, 25*, 1105–1117.

Kocsis, A., & Challamel, N. (2016). On the post-buckling of distributed microstructured system: The finite element elastica. *International Journal of Mechanical Sciences, 114*, 12–20.

Lakes, R. (Ed.), (2020). *Composites and metamaterials*. Singapore: World Scientific.

Leahu-Aluas, I., & Abed-Meraim, F. (2011). A proposed set of popular limit-point buckling benchmark problems. *Structural Engineering and Mechanics, 38*(767).

Li, Z., & Zheng, J. (2019). Nonlinear buckling mechanism of an arch subjected to a symmetrically-placed point load. *KSCE Journal of Civil Engineering, 23*, 4781–4789.

Luongo, A., Ferretti, M., & Di Nino, S. (2023). *Stability and bifurcation of structures: statical and dynamical systems*. Cham: Springer.

Makowski, J., & Stumpf, H. (1986). Finite strains and rotations in shells. In W. Pietraszkiewicz (Ed.), *Finite rotations in structural mechanics* (pp. 175–194). Berlin, Heidelberg: Springer.

Malikan, M., Krasheninnikov, M., & Eremeyev, V. A. (2020). Torsional stability capacity of a nano-composite shell based on a nonlocal strain gradient shell model under a three-dimensional magnetic field. *International Journal of Engineering Science, 148*, Article 103210.

Mises, R. V. (1923). Über die stabilitätsprobleme der elastizitätstheorie. *ZAMM-Journal of Applied Mathematics and Mechanics/Zeitschrift für Angewandte Mathematik und Mechanik, 3*, 406–422.

Nolte, L.-P., & Chróścielewski, J. (1986). Large rotation elastic–plastic analysis of flexible shells. In C. Taylor, & et al. (Eds.), *Numerical methods for non-linear problems, Vol. 3* (pp. 391–404). Swansea: Pineridge Press.

Nolte, L.-P., Makowski, J., & Stumpf, H. (1986). On the derivation and comparative analysis of large rotation shell theories. *Archive of Applied Mechanics, 56*, 145–160.

Ong, O. Z. S., Ghayesh, M. H., & Losic, D. (2023). Vibrations of porous functionally graded CNT reinforced viscoelastic beams connected via a viscoelastic layer. *International Journal of Engineering Science, 191*, Article 103917.

Ostoja-Starzewski, M. (2002). Lattice models in micromechanics. *Applied Mechanics Reviews, 55*, 35–60.

Penna, R. (2023). Bending analysis of functionally graded nanobeams based on stress-driven nonlocal model incorporating surface energy effects. *International Journal of Engineering Science, 189*, Article 103887.

Peraza Hernandez, E. A., Hartl, D. J., & Lagoudas, D. C. (2019). *Active origami: modeling, design, and applications*. Cham: Springer.

Perelmuter, A. V., & Slivker, V. (2013). *Handbook of mechanical stability in engineering. 1: genral theorems and individual members of mechanical systems*. New Jersey: Worlld Scientific.

Pi, Y.-L., Bradford, M. A., & Guo, Y.-L. (2016). Revisiting nonlinear in-plane elastic buckling and postbuckling analysis of shallow circular arches under a central concentrated load. *Journal of Engineering Mechanics, 142*, Article 04016046.

Pignataro, M., Rizzi, N., & Luongo, A. (1991). *Stability, bifurcation and postcritical behaviour of elastic structures, Vol. 39*. Amsterdam: Elsevier.

Reissner, E. (1972). On one-dimensional finite-strain beam theory: the plane problem. *Zeitschrift für Angewandte Mathematik und Physik ZAMP, 23*, 795–804.

Rezaiee-Pajand, M., & Rajabzadeh-Safaei, N. (2022). Stress-driven nonlinear behavior of curved nanobeams. *International Journal of Engineering Science, 178*, Article 103724.

Roudbari, M. A., Jorshari, T. D., Lü, C., Ansari, R., Kouzani, A. Z., & Amabili, M. (2022). A review of size-dependent continuum mechanics models for micro-and nano-structures. *Thin-Walled Structures, 170*, Article 108562.

Simmonds, J. (2010). A simple energetic explanation of the polygon-circle paradox for classical (Kirchhoff) plate theory. *Journal of Elasticity, 99*, 113–116.

Simo, J. C., Hjelmstad, K. D., & Taylor, R. L. (1984). Numerical formulations of elasto-viscoplastic response of beams accounting for the effect of shear. *Computer Methods in Applied Mechanics and Engineering, 42*, 301–330.

Simo, J. C., & Vu-Quoc, L. (1986). A three-dimensional finite-strain rod model. Part II: Computational aspects. *Computer Methods in Applied Mechanics and Engineering, 58*, 79–116.

Simo, J. C., Wriggers, P., Schweizerhof, K. H., & Taylor, R. L. (1986). Finite deformation post-buckling analysis involving inelasticity and contact constraints. *International Journal for Numerical Methods in Engineering, 23*, 779–800.

Stumpf, H., & Makowski, J. (1987). On large strain deformations of shells. *Acta Mechanica, 65*, 153–168.

Taloni, A., Vilone, D., & Ruta, G. (2023). General theory for plane extensible elastica with arbitrary undeformed shape. *International Journal of Engineering Science, 193*, Article 103941.

Thompson, J. M. T., & Hunt, G. W. (1973). *A general theory of elastic stability*. London: Wiley.

Timoshenko, S. P., & Gere, J. M. (1963). *Theory of elastic stability* (2nd ed.). Auckland: McGraw-Hill.

Turco, E. (2018). Discrete is it enough? The revival of Piola–Hencky keynotes to analyze three-dimensional elastica. *Continuum Mechanics and Thermodynamics, 30*, 1039–1057.

Turco, E., Barchiesi, E., Giorgio, I., & DellIsola, F. (2020). A Lagrangian Hencky-type non-linear model suitable for metamaterials design of shearable and extensible slender deformable bodies alternative to Timoshenko theory. *International Journal of Non-Linear Mechanics, 123*, Article 103481.

Vaccaro, M. S. (2022). On geometrically nonlinear mechanics of nanocomposite beams. *International Journal of Engineering Science, 173*, Article 103653.

Vorovich, I. I. (1998). *Nonlinear theory of shallow shells, Vol. 133*. New York: Springer.

Wang, S., Ding, W., Li, Z., Xu, B., Zhai, C., Kang, W., Yang, W., & Li, Y. (2023). A size-dependent quasi-3D model for bending and buckling of porous functionally graded curved nanobeam. *International Journal of Engineering Science, 193*, Article 103962.

Wang, T., Liu, F., Fu, C., Zhang, X., Wang, K., & Xu, F. (2021). Curvature tunes wrinkling in shells. *International Journal of Engineering Science, 164*, Article 103490.

Wang, C. M., Wang, C. Y., & Reddy, J. N. (2005). *Exact solutions for buckling of structural members*. CRC Press.

Waszczyszyn, Z. (1983). Numerical problems of nonlinear stability analysis of elastic structures. *Computers and Structures, 17*, 13–24.

Wriggers, P. (2017). The art of modeling in solid mechanics. In F. Pfeiffer, & H. Bremer (Eds.), *The art of modeling mechanical systems* (pp. 321–386). Cham: Springer International Publishing.

Wriggers, P., & Simo, J. C. (1990). A general procedure for the direct computation of turning and bifurcation points. *International Journal for Numerical Methods in Engineering, 30*, 155–176.

Yang, W., Wang, S., Kang, W., Yu, T., & Li, Y. (2023). A unified high-order model for size-dependent vibration of nanobeam based on nonlocal strain/stress gradient elasticity with surface effect. *International Journal of Engineering Science, 182*, Article 103785.

Yee, K., & Ghayesh, M. H. (2023). A review on the mechanics of graphene nanoplatelets reinforced structures. *International Journal of Engineering Science, 186*, Article 103831.

Zhang, H., Challamel, N., Wang, C., & Zhang, Y. (2019). Buckling of multiply connected bar-chain and its associated continualized nonlocal model. *International Journal of Mechanical Sciences, 150*, 168–175.